Journal of Nuclear Materials 543 (2021) 152586

Contents lists available at ScienceDirect

Journal of Nuclear Materials

journal homepage: www.elsevier.com/locate/jnucmat

UPDATED U3SI2 thermal creep model and sensitivity analysis of the U3SI2-SIC accident tolerant FUEL

J.A. Yingling [a,*], K.A. Gamble [b], Elwyn Roberts [a], R. Austin Freeman [a], Travis W. Knight [a]

[a] University of South Carolina, Mechanical Engineering Department, Columbia, SC 29208
[b] Idaho National Laboratory, Fuel Modeling and Simulation, Idaho Falls, ID 83415

ARTICLE INFO

Article history:
Received 6 July 2020
Revised 16 September 2020
Accepted 3 October 2020
Available online 9 October 2020

Keywords:
Multi-physics simulation
Nuclear fuel performance
Pellet-cladding mechanical interaction
Uranium silicide
U3si2
Silicon carbide
Sic
Thermal creep

ABSTRACT

U_3Si_2 is a candidate accident tolerant fuel (ATF) replacement for UO_2. U_3Si_2's high uranium density and high thermal conductivity are favorable properties in steady-state and accident conditions. Low power performance of this U_3Si_2-SiC concept fuel is compared to that of UO_2-Zr4 fuels by implementing models that describe the properties of U_3Si_2 and SiC-SiC into Idaho National Laboratory's (INL) fuel performance code, BISON. Included in these material models is a thermal creep model for U_3Si_2 based on compressive creep data. The simulated results are in keeping with community knowledge that the U_3Si_2-SiC concept fuel may serve as a replacement for UO_2-Zr4 fuels during steady-state operation, provided the mSiC layer remains under compression. Through a moderate power history and three 24-month fuel cycles, the mSiC layer remains under compressive stress through a burnup of 80 MWd/kgU. During low power operation, failure of the mSiC layer generally occurs prior to significant thermal creep in U_3Si_2. Generally, U_3Si_2 creep is temperature sensitive and of little importance at the temperatures and stresses simulated during steady operation and during fuel-to-cladding contact. A parameter variation study including 11,520 individual simulations with variations in nominal fuel thermal creep rate, cladding thermal conductivity, cladding irradiation creep and swelling, cladding gap size, and cladding thickness demonstrated that research priorities for this ATF should revolve around reducing cladding thickness as a means to minimize cladding failure. Generally, despite advances in SiC-SiC compliance, the brittle nature of mSiC excludes U_3Si_2-SiC for use where fuel cladding contact may occur.

1. Introduction

1.1. Motivation

The goal behind accident tolerant fuel (ATF) research is to replace standard light water reactor (LWR) fuel with a fuel that lessens the severity of accidents while maintaining or improving fuel performance [1]. Amongst the candidates for ATFs, uranium silicide (U_3Si_2) is of interest due to its high uranium density and high thermal conductivity. Although corrosion of U_3Si_2 with water, along with a low melting point, phase complexity and interactions with SiC cladding [2], have recently reduced enthusiasm for its use in accident tolerance, recent works continue its evaluation [3] and have shown favorable accident performance in recent computational studies [4]. Additionally, much of the high burnup in-reactor behavior of U_3Si_2 is not known [5]. Specifically, an experimentally derived model describing the thermal creep of U_3Si_2 is lacking in the literature. This work reports the development of a thermal creep model for U_3Si_2 based on compressive creep experiments performed at the University of South Carolina (UofSC) [6,7] and demonstrates its effects via finite element simulation.

Replacements for Zircaloy cladding are desired to lengthen the time nuclear operators have to respond to accidents. SiC is under consideration as a cladding material due to its high strength, minimal thermal and irradiation creep, high steam oxidation resistance, and minimal neutron economy penalty [8]. However, due to its brittle nature, monolithic SiC (mSiC) is not suitable for single layer cladding applications and a composite matrix ceramic SiC (SiC-SiC) must be used to allow more gradual failure modes [9]. While the use of SiC-SiC improves the mechanical compliance of a SiC cladding, stresses in the mSiC layer used as an environmental barrier must remain below the threshold for microcracking to avoid the release of fission gasses into the coolant [10].

Recent works indicate that SiC claddings require significant development prior to use. He et al. [11] evaluated the failure probability of U_3Si_2 with duplex SiC cladding and found SiC failure to be almost certain under reactivity insertion accident (RIA) conditions.

* Corresponding author: Address: University of South Carolina, 300 Main Street, Columbia, SC 29208
E-mail address: jacobay@email.sc.edu (J.A. Yingling).

https://doi.org/10.1016/j.jnucmat.2020.152586
0022-3115/

Table 1
Summary of UofSC compressive creep experiments.

Pellet ID	Test #	Creep Rate (1/s)	Average Temperature (K)	Temperature Variation (Std. dev/μ)	Average True Stress (MPa)	Stress Variation (Std. dev/μ)	Time (Hrs)	Grain Size (μm) [17]
150,813-A	1	8.7327E-8	1218.37	0.017	44.10	0.034	100	15.6
	2	1.1342E-7	1205.18	0.019	71.77	0.016	100	15.6
	3	N/A	N/A	N/A	N/A	N/A	N/A	N/A
150,813-B	4	1.7042E-8	1121.22	0.060	77.66	0.021	433	15.6
	5-A	1.3081E-7	1223.89	0.090	65.13	0.029	105	15.6
	5-B	6.4806E-8	1210.07	0.010	57.71	0.024	200	15.6
161,214-B	6	1.5728E-8	1173.59	0.000	46.43	0.009	230	26
	7	4.6342E-8	1223.59	0.000	45.21	0.014	230	26
161,214-A	8	1.5486E-8	1223.60	0.000	29.51	0.013	65	26
	9	2.7472E-8	1223.53	0.000	49.73	0.012	135	26
	10	7.1920E-8	1223.64	0.000	63.62	0.006	82	26
161,214-C	11	1.1171E-8	1223.69	0.000	26.91	0.020	280	26
	12	1.8750E-8	1273.61	0.000	26.45	0.021	330	26
	13	2.9831E-8	1273.61	0.000	47.79	0.010	140	26

Using BISON, Wei [12] calculated elevated cladding hoop stresses greater than 180 MPa during shutdown which is enough to exceed its proportional limit stress (PLS) [13]. After surpassing the PLS, the resulting microcracking in the SiC-SiC can result in fission gas leakage, leaving the relatively more brittle mSiC as the only hermetic barrier. This is exceptionally problematic since rapid failure of mSiC cladding is known to occur following pellet cladding mechanical interaction (PCMI) even when pseudoplastic compliance of the composite layer is considered [6].

Since the magnitude of U_3Si_2 creep is directly related to cladding stress during contact, accurate prediction of SiC cladding failure in U_3Si_2-SiC simulations requires investigation of an improved thermal creep model. Until now, simulations of this concept fuel were completed using Metzger's U_3Si_2 thermal creep model [11], which was developed using Finlay's irradiation and swelling data [14], with kinetic theory [10]. The development of an experimentally derived thermal creep model enhances understanding of the U_3Si_2-SiC fuel system to help identify fuel design priorities.

1.2. Objectives

In this work, the BISON nuclear fuel performance code is used to further understanding of the U_3Si_2-SiC ATF concept by: (1) developing a full physics simulation for the U_3Si_2-SiC ATF concept, including the experimentally derived thermal creep model developed in this work and the various U_3Si_2 and SiC models of the open literature, (2) providing a predictive comparison of the concept ATF against UO_2-Zr4 fuels, and (3) identifying essential U_3Si_2-SiC ATF design priorities through parameter variation studies to test simulation response to variations in U_3Si_2 thermal creep, SiC thermal conductivity, cladding gap, and SiC-SiC cladding layer thickness.

2. U3Si2 thermal creep

2.1. Model data

UofSC thermal creep data [15] is fit using the Mukherjee-Bird-Dorn equation [16]:

$$\dot{\epsilon} = \frac{AGb}{kT}\left(\frac{b}{d}\right)^m \left(\frac{\sigma}{G}\right)^n D_0 e^{-\frac{Q}{RT}} \quad (1)$$

$$\dot{\epsilon} = \frac{A'}{T}\frac{\sigma^n}{d^m} e^{-\frac{Q}{RT}} \quad (2)$$

Eq. (1) is an empirical secondary thermal creep model capable of accounting for dislocation and diffusional components through its incorporation of stress, temperature, and grain-size-dependent factors. Due to uncertainties in the original experiment, primary thermal creep of U_3Si_2 was unable to be determined reliably and is excluded from the model [7]. Eq. (1) is simplified by collecting leading factors into a single coefficient (A'). When Eq. (2) is rearranged, the coefficients A' and Q are found by iterating over values of m and n to calculate a linear least squares fit of $\ln(\varepsilon T d^m \sigma^{-n})$ against T^{-1}.

Table 2
Creep parameters for Eq. (2).

A'	n	m	Q (kJ/mol K)
4.841e-19	1.936	1.86	223.1

UofSC received various batches of U_3Si_2 pellets for characterization and creep testing. The data received from INL for determining U_3Si_2 creep coefficients came from compressive creep trials from Batches 3 and 4 [15]. The compressive creep experiment covered a range of temperatures and stresses applicable to LWR conditions. A total of 13 creep tests were conducted on five U_3Si_2 pellets. Tests 1-5 use pellets from Batch 3, and Tests 6-13 use pellets from Batch 4. Table 1 above provides the average results of these experiments after applying statistical controls to minimize error when calculating secondary creep for each test [6,7].

2.2. Model parameters

The average strain rates, temperatures, and true stresses in Table 1 were calculated based on the following requirements: (1) Include a range of data for at least 65 h of steady-state creep time outside of the first 130 h to allow sample seating and any primary creep to complete. (2) The experimental average strain rate for this range of data must have a coefficient of correlation (r^2) greater than 0.90. (3) The average temperature and true stress for the range of data must have a coefficient of variation ($\sigma\mu^{-1}$) less than 0.035 to minimize variations in the calculated means.

2.3. Experimental variations

Fig. 1 shows the overlap between the measured and calculated strain rates using Eq. (2) as a secondary creep model. In Table 2, U_3Si_2 creep coefficients for Eq. (2) are found by iterating over values of m between 0 and 5, and of n between 1 and 7 until the highest r^2 is found. The Q and A' creep parameters are found from the slope and intercept of the best fit, respectively. The error bars in Fig. 1 are determined by propagating the experimental data variations in temperature and stress through the creep model in Eq. (2). In addition to these experimental variations, a 2% systematic

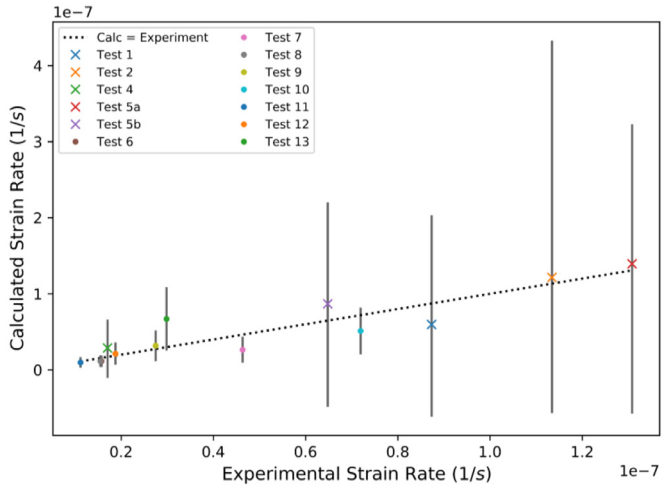

Fig. 1. Calculated model vs experimental data (p-value=0.00002, r^2=0.83).

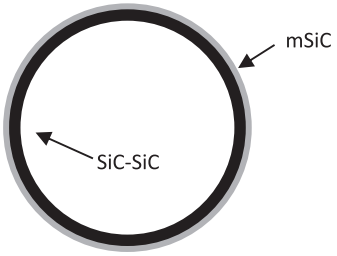

Fig. 2. Duplex cladding arrangement.

variation in the temperature and stress measurements is assumed to account for bias due to measurement technique. Consequently, the combined effect of temperature and stress variations on the calculated creep rate is evident.

The grain size used in the creep calculations are from Table 1 and were determined from pre-creep batch samples using ImageJ software [17]. Experimental variations in grain size were omitted from the error propagation in Fig. 1, since the time-dependent evolution of grain size throughout creep testing is unknown. However, post-creep sample grain sizes were evaluated at UofSC, and found that grain growth of a few microns had occurred, particularly among higher temperature creep specimen [18]. This is in line with expectations from recent U_3Si_2 grain growth models which show much less grain growth in U_3Si_2 than UO_2 near the tested creep temperatures [19].

Among these data, Tests 1–5 are notable for their pronounced propagated error. This error sources from the lack of PID temperature control early in the UofSC creep experiment [7]. These data points cannot be excluded from the model as they contain the entirety of Batch 3 creep specimen and their different grain size necessary to the development of the model. As indicated by the proximity of the model calculated means, it is believed that the statistical controls given in Section 2.2 have adequately isolated the mean creep rate for these Tests despite the noise inherently in the data.

When the creep parameters of Table 2 are used in Eq. (2) and plotted against the experimental values of Table 1, we observe that the data fit to the model within the range of calculated variations. A notable exception is the calculated strain rate for Test 7, which is unable to match measured experimental values. This discrepancy is explained by the misalignment of Sample 161,214-B, which resulted in excessive sample curvature and non-uniform compressive stress during the later stage of the test [7]. Since the experimental strain rate measurement depends on uniaxial stresses, the non-uniform stress condition may have caused heightened stress along a pellet edge, resulting in an erroneously high strain rate measurement. However, considering the overall variations in the experimental data and the generally low thermal creep rate, the errors in Test 7 do not seem large enough to warrant exclusion from the model.

3. BISON material models

3.1. Model summary

Finite element analysis methods were used to determine the impact of the developed U_3Si_2 secondary thermal creep model on the performance of the ATF concept. BISON is a finite element analysis code described by others throughout the development of fuel performance models [20,21]. Table 3 summarizes the material models used in the U_3Si_2-SiC, UO_2-SiC, and UO_2-Zr4 BISON simulations. Bold italicized cells represent models either added to the BISON codebase or modified from their original format. Models that have been modified are described in Section 3.2. Unitalicized cells are material models already available in BISON version 1.5. Coefficient values for generic material models are provided using standard symbols and assuming SI units.

The rod geometry is a duplex SiC cladding that follows the outside monolithic design as suggested by Stone to reduce overall failure probability [26]. Stone found that this cladding arrangement ensured compression of the outer mSiC throughout fuel life. By maintaining the outer mSiC in compression, concerns regarding SiC-SiC cracking and loss of hermeticity are lessened. Geometry specifics such as rodlet length and diameter, cladding gap, and cladding layer thicknesses are found in Section 4.1.

3.2. Model development and modification

3.2.1. Thermal expansion of U_3Si_2

Obbard et al. [22] describe the linear coefficient of thermal expansion of U_3Si_2 as Eq. (3). Since BISON has existing thermal expansion models in place, Obbard's linear thermal expansion coefficient function was added to the existing code as an option.

$$\alpha(\mathrm{T}) = 2.10 \cdot 10^{-5} - 7.25 \cdot 10^{-9}\mathrm{T} \tag{3}$$

3.2.2. SiC-SiC thermal conductivity

Irradiation damage of SiC is an important part of describing its thermal conductivity. SiC-SiC is modeled by adding Stone's irradiation damage resistivity model to Koyanagi's unirradiated tube specimen thermal diffusivity data in the following manner:

$$k_{nonirr} = \alpha \rho C_p \tag{4}$$

$$R_{nonirr} = k_{nonirr}^{-1} \tag{5}$$

$$R_{irr} = 15.11 \cdot S \tag{6}$$

$$k_{tot} = \frac{1}{R_{irr} + R_{nonirr}} \tag{7}$$

Density (ρ), thermal diffusivity (α), and specific heat (C_p) data for Eq. (4) are taken from Koyanagi [27]. Resistivity due to irradiation in Eq. (6) is taken from Stone [26]. Non-irradiative thermal resistivity is added to irradiative thermal resistivity in Eq. (7) to determine a combined coefficient of thermal conductivity for tubular SiC-SiC.

Li, et al. have implemented a mechanical damage model that severely degrades SiC-SiC thermal conductivity as a function of

Table 3
Material models used in BISON simulation.

	UO_2	U_3Si_2	Monolithic SiC	Composite SiC	Zircaloy-4
Thermal Expansion	α=10e-6	*Obbard* [22]	Katoh [23]	Katoh [23]	
Specific Heat	NFIR [24]	White [25]	Stone [26]	Koyanagi [27]	C_p=330
Thermal Conductivity	NFIR [24]	White [25]	Stone [26]	*Koyanagi* [27] *modified*	k=16
Swelling	SIFGRS [28]	Barani [29], Hofmann [30]	Katoh [31]	Katoh [31]	Franklin [32]
Fission Gas Release	SIFGRS [28]	Barani [29]	N/A	N/A	N/A
Elasticity	E=2e11 ν=0.345	White [25]	*Snead* [33] *modified*	*Singh* [34] *modified*	E=7.5e10 ν=0.3
Plasticity	N/A	N/A	N/A	*Data from Braun* [35]	N/A
Creep	Allison [36]	*This work (Thermal)*	*Koyanagi* [37] [38]	*Koyanagi* [37] [38]	Limback-Hoppe [39]
Fracture/Relocation	Fancher [40]	*Fancher* [40] *modified*	N/A	N/A	N/A
Densification	Fancher [40]	None [5]	N/A	N/A	N/A

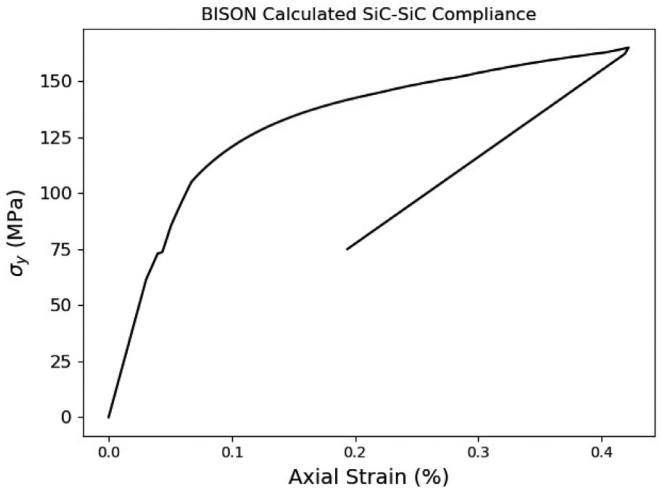

Fig. 3. Simulated SiC-SiC pseudoplasticity.

maximum strain and relaxed strain conditions in the cladding [41]. Although such a model was developed, it wasn't committed back to the BISON framework and was unavailable within BISON at the time of this study. The SiC-SiC mechanical damage model development by Li, et al. is important to the BISON users that are studying U3Si2-SiC and would make a valuable addition to the framework. Since mechanical degradation of SiC-SiC thermal conductivity was not included in our nominal simulation, a variation in SiC-SiC thermal conductivity is included in Section 4.5 to demonstrate simulation sensitivity to variations in thermal conductivity.

3.2.3. SiC elasticity

Many of SiC's properties are affected by irradiation damage. This damage is completed prior to 2 dpa of fluence [31]. To account for the irradiation degradation of the elastic modulus, mSiC and SiC/SiC are modeled to linearly degrade the value of the elastic modulus from 460 GPa [33] and 201.9 GPa [42] by 10% and 18.4%, respectively, over 2 dpa [43].

3.2.4. SiC-SiC compliance

Composite matrix ceramic (CMC) materials have an elastic modulus that varies based on a stress-dependent damage coefficient. Braun et al. determined the damage coefficient for SiC-SiC via axial applied stresses [35]. To model this behavior, the elastic modulus for SiC-SiC was damaged proportional to the damage coefficient calculated from Braun's results. In Fig. 3, by ramping axial stress up to 165 MPa, and then down to 75 MPa, the correct pseudoplastic behavior of this model is verified on a simple SiC-SiC geometry. Since Braun's damage coefficient is highly sensitive to cladding stress, a specialized time-stepping routine was added to BISON which ensures an adequately small change in the damaged modulus between time steps.

3.2.5. SiC irradiation creep

Creep of mSiC and SiC-SiC under irradiation is relatively small and is described by Koyanagi's bend stress ratio (BSR) experiments as having a swelling coupled primary creep region as well as a steady-state secondary creep [37]:

$$\dot{\varepsilon}_{\text{tot}} = \dot{\varepsilon}_{\text{pri}} + \dot{\varepsilon}_{\text{sec}} \tag{8}$$

Primary irradiation creep is coupled to volumetric swelling, $\dot{\varepsilon}_{vol}$, through a creep compliance coefficient [34]:

$$\text{K}_{\text{pri}} = \left(3.5626 \cdot 10^{-4}\text{T}^2 - 4.1704 \cdot 10^{-1}T + 156.8507\right)\ \text{TPa}^{-1} \tag{9}$$

$$\dot{\varepsilon}_{\text{pri}} = \text{K}_{\text{pri}}\sigma\,\dot{\varepsilon}_{\text{vol}} \tag{10}$$

Secondary irradiation creep is proportional to stress and fluence [44], with a compliance coefficient of approximately $K_{sec} = 1 \cdot 10^{-7}(\text{MPa dpa})^{-1}$ [37]:

$$\dot{\varepsilon}_{sec} = K_{sec}\sigma\phi \tag{11}$$

Since the BSR technique only represents SiC creep qualitatively, Koyanagi quantitatively calculated the stress and irradiation damage normalized creep strain for in-reactor CVD SiC tubes [38]. These creep data have shown in-pile creep rates to be between 2 and 17 times higher than BSR estimates. In the parameter variation study in Section 4.4, a scaling factor is introduced to the total creep rate to account for this range of irradiation creep.

3.2.6. Fuel fracture and relocation

U_3Si_2 lacks a developed model to describe its fracture and subsequent relocation during rise to power. Li, et al. have also studied the U_3Si_2-SiC concept without a fracture and relocation model [41]. However, fuel fracture and relocation are important for accurately describing fuel stress and strain during simulation, without which unrealistically high fuel stresses may be calculated. A recent post-irradiation examination of U_3Si_2 at INL shows that through 20 MWd/kgU of burnup U_3Si_2 exhibits about 25% of the cracking UO2 would experience under the same conditions [5]. In the absence of a validated cracking model, this work uses the UO_2 ESCORE model already available in BISON but reduced by a factor of 0.25 as a first approximation. Simulation impact from variations in this factor is studied in the multidimensional parameter variation study hereafter.

3.2.7. Densification and U_3Si_2 thermal conductivity degradation

The material models of the present U_3Si_2-SiC simulation differ from those used by He, et al. through the incorporation of the material model improvements indicated in Sections 3.2.1–3.2.6 above. Other notable differences include fuel densification and thermal conductivity degradation. He et al. assumes densification is similar to UO_2 [11]. However, since post-irradiation examination indicates that fuel porosity is not impacted at low burnup [5], and that densification is largely a phenomenon evident at low burnups, densification in U_3Si_2 is not considered in this study. Additionally, He et

Table 4
Simulation conditions.

Cycle Linear Heat Rate	21.16, 19.3, 17.5 kW/m (three 24-month cycles)
Initial Plenum Pressure	2 MPa
Coolant Pressure	15.31 MPa
Coolant Inlet Temperature	599.95 K
Coolant Flow Rate	3675.4 kg/(m^2–*sec*)
Rodlet Pitch	12.6 mm
Rodlet Radius	4.75 mm
Fuel-to-Cladding Gap	80 μm
SiC/SiC Thickness	0.6 mm
mSiC Thickness	0.2 mm
Zircaloy Thickness	0.572 mm
Fuel Height (10 pellets)	9.8 cm
Plenum Height	10.38 cm
U_3Si_2 Grain Size	20 μm

al. assume that U_3Si_2 thermal conductivity degrades by 50% over 60 MWd/kgU. Considering the porosity observations given above, this assumption is likely excessive. Since irradiated material properties for U_3Si_2 are sparse in the literature [25], this work makes use of the U_3Si_2 handbook's empirical relation with no thermal conductivity degradation.

3.2.8. Parameter variation study

Uncertainties in material models can lead to wide variations in model predictions. The ability to perform parametric studies on multiple models at the same time is of interest. Coupling BISON to the Dakota software [45] developed at Sandia National Laboratories (SNL) allows for rapid turnaround on parametric studies that can contain many uncertain inputs. Given that parametric studies include discrete values for the uncertain inputs, a multidimensional parameter study can be performed where all possible combinations of input values are investigated. This means multiple parameters may be perturbed at the same time. The results of multidimensional parameter studies can be plotted in what are known as main effects plots, which provide insight into the influence of particular uncertain inputs on output metrics of interest while taking into account the influence of other inputs at the same time. Other examples of using such a method (i.e., coupling BISON to Dakota) for parametric studies for investigating the behavior of materials where limited experimental data is available can be found in the literature [46,47].

4. Results and discussion

4.1. Simulation conditions

The default models in BISON and those developed above are implemented in simulations to provide a comparative view of the performance differences in three cases: (1) UO_2-Zr4, (2) UO_2-SiC, and (3) U_3Si_2-SiC. The simulation conditions used for this comparison are shown in Table 4 below.

The simulation geometry is a single short rod (rodlet) with a smeared fuel mesh of 588 QUAD8 elements. To aid with the contact algorithm, the SiC-SiC and mSiC meshes are more fine with 320 and 240 elements respectively. Several mesh refinements were tested and found to be unnecessary as they produce similar results at greater computational expense. The contact model employed was frictionless and was deemed sufficient for the present study considering frictionless models have been used successfully in many BISON validation tests [48]. Additionally, BISON validation of PCMI has shown that friction contact models with variations in friction coefficient ranging from nearly frictionless to nearly glued, μ=(0.1–1000), are very similar in outcome [49]. External geometry, coolant flow rate, inlet temperature, and pressure in the three simulations are identical.

Since the simulated geometry is much shorter in length than a typical commercial fuel rod, coolant temperature rise through the channel is much less than it would be otherwise. To compensate for this, the inlet coolant temperature and coolant flux were specified at the most constraining nominal channel values for a Seabrook pressurized water reactor [50]. That is, inlet coolant temperature was set conservatively high, and coolant mass flux was set conservatively low. In this way the simulated results are intended to bound fuel performance in the limit of high temperature while under moderate power and steady operation.

Since much of the motivation behind using U_3Si_2-SiC is economic, a moderate power history was chosen to facilitate 24-month fuel cycles. To accomplish this, a maximum operating power density of 40 W/gU is specified [51]. This requirement limits the linear heat generation rate (LHGR) to 21.16 kW/m in the first cycle. Startups and shutdowns occur linearly over a 24 hour period. Relatively small decreases in power were chosen between cycles to approximate a simple power history in the absence of burnable poisons and subsequent moving of the rod to locations in the core of lower neutron flux. Linear heat rates for subsequent cycles are chosen to bring the average burnup of the simulated rodlet to 80MWd/kgU after three 24 month cycles.

The reader is advised that such high burnups are likely not possible due to U_3Si_2's additional uranium fraction alone. For reference, recent UO_2-Zr4 PWR studies using 24-month cycles are limited to two cycles and a discharge burnup of near 60MWd/kgU [52]. Although attainment of such a large burnup may not be possible without enrichment beyond 5%, the thermal-mechanical results of this study do not depend upon the enrichment of the fuel. Additionally, exploration of thermo-mechanical performance beyond known attainable burnups is essential as many advanced reactor concepts depend on enrichments greater than 5%, a fact of recent exploration by Burns et al. [53].

4.2. Simulation end criteria

Each simulation case was run until one of two possible outcomes occurred: (1) Cladding failure criteria was reached, as discussed below or (2) the target average fuel burnup of 80MWd/kgU was achieved. An average fuel burnup of 80 MWd/kgU was selected as the goal average burnup in this work. Since equally enriched UO_2 fuels are capable of more than 60MWd/kgU, the selection of 80MWd/kgU was a burnup goal based on the higher uranium density of U_3Si_2 [54].

4.2.1. Cladding failure criteria

Cladding failure for U_3Si_2-SiC is defined as reaching a maximum mSiC cladding hoop stress of 173 MPa, the average characteristic failure stress of mSiC determined by Deng [55]. Zr4 cladding failure was taken as an irradiated hoop strain limit, determined by Jernkvist to be 1.3% [56]. These measures of failure are sampled from the entire cladding in the case of Zr4, but only from the monolithic portion of the cladding in the case of SiC.

4.3. Simulation response

4.3.1. Fuel temperature

In Fig. 4, maximum, average, and minimum temperatures were calculated to indicate the temperature distribution in the fuel to high burnup. Maximum homologous temperatures (T_{max}/T_m) with melting points of 3138 K and 1938 K for UO_2 and U_3Si_2, respectively, were calculated to indicate the margin to melt within each fuel.

Although the U_3Si_2-SiC fuel concept has lower maximum fuel temperatures, it operates at a higher homologous temperature

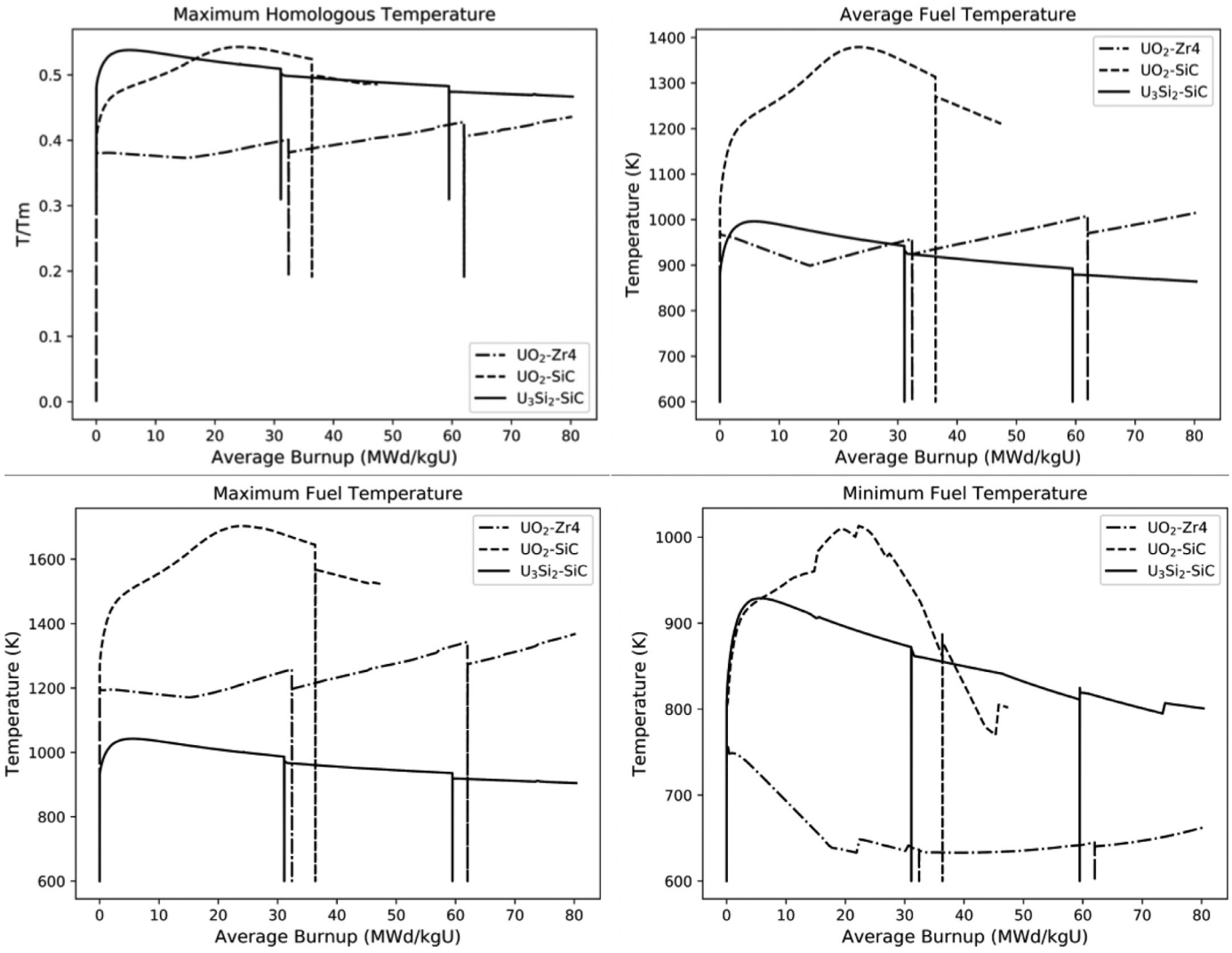

Fig. 4. Fuel temperature as a function of average burnup.

(T_{max}/T_m). Irradiative degradation of the SiC cladding is responsible for the large increase in temperature at low burnup. This effect is particularly evident in the case of U_3Si_2-SiC in which the startup T_{max}/T_m increases to above 0.5 during the first 10 MWd/kgU. Clearly, although U_3Si_2-SiC generally has a lower steady-state maximum operating temperature, its margin to melt is much lower than that of UO_2-Zr4 since T_{max}/T_m remains much higher than UO_2-Zr4 for the entire simulation. Unfortunately, from the perspective of margin to fuel melt, U_3Si_2-SiC seems to provide no additional accident tolerance than the status quo.

Performance of UO_2-SiC is substantially worse than the other fuels and only reaches about 50 MWd/kgU before the failure criteria for the SiC cladding has been reached. It is noteworthy that, after accounting for differences in power density, cladding thickness, and units of burnup; the temperatures and delay in cladding contact in this simulation is comparable to those seen by Singh et al. [57]. While the UO_2-SiC simulation ends in the event of cladding failure, U_3Si_2-SiC and UO_2-Zr4 perform identically in this regard as the simulations ran to completion without cladding failure. While U_3Si_2-SiC appears to have some minor benefit at high burnup, in view of the temperature performance shown in Fig. 4, it is hard to recommend U_3Si_2-SiC as a replacement for UO_2-Zr4.

The chosen nominal power history is conservative to allow the use of 24-month cycles. However, since the ability to effectively conduct heat at higher temperatures is an advantage of U_3Si_2 fuel, two additional power densities were simulated to explore the extent of U_3Si_2-SiC's acceptable power limits. Fig. 5 below, shows a comparison between the nominal case, 25% and 50% higher power.

U_3Si_2's thermal conductivity allows for significant increases in power at the expense of very little decrease in margin to melt. However, despite this advantage, the 25% and 50% power increases both resulted in cladding failure at 68 and 38 MWd/kgU, respectively. At typical core power, peak power densities of more than 30 kW/m are common for steady-state lead PWR rods. For example, the full core U_3Si_2-SiC simulation of He, et al. found maximum LHGR to be 35.5 kW/m [11]. In light of this, Fig. 5 indicates that U_3Si_2-SiC would certainly fail at these powers and cannot be recommended for high-power applications without increases in cladding gap or other modification of the design. These results suggest that limiting LHGR to less than 25 kW/m is necessary to prevent contact and avoid premature cladding failure.

4.3.2. Plenum pressure and fission gas release

There is no validated fission gas release (FGR) model for U_3Si_2; however, the FGR model developed by Barani et al. [29] demonstrates what is generally expected from U_3Si_2 based on rate parameters informed by density functional theory. In Fig. 6, the results show no FGR through 80 MWd/kgU. Although, the high-burnup

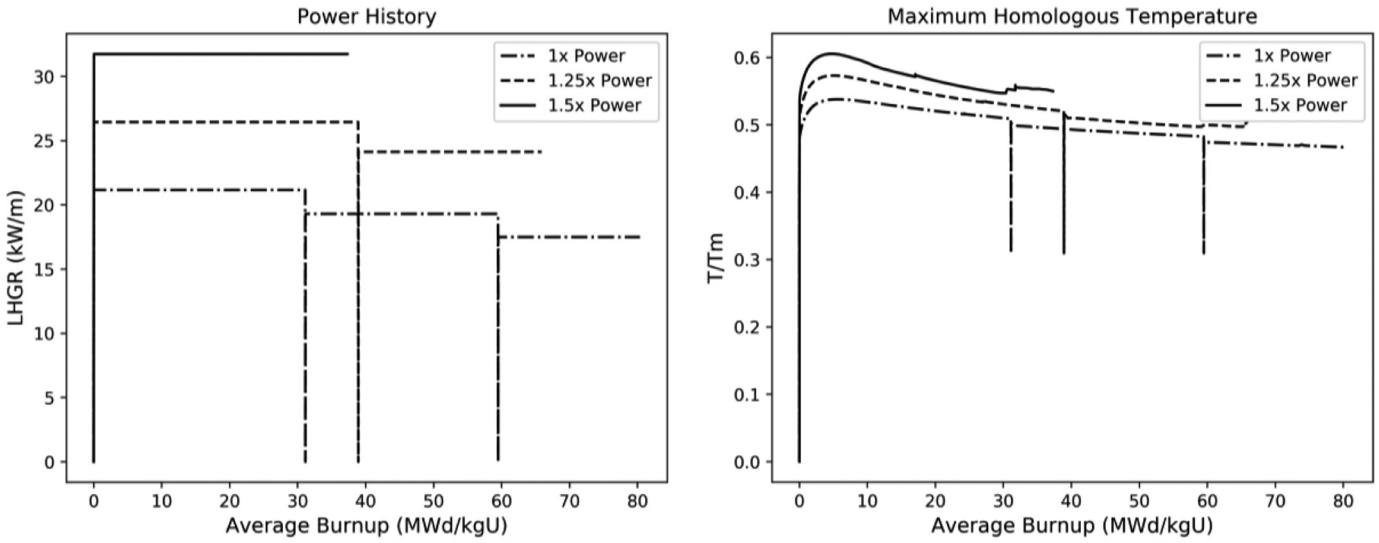

Fig. 5. Fraction of melting point in U_3Si_2-SiC for increasingly higher power density.

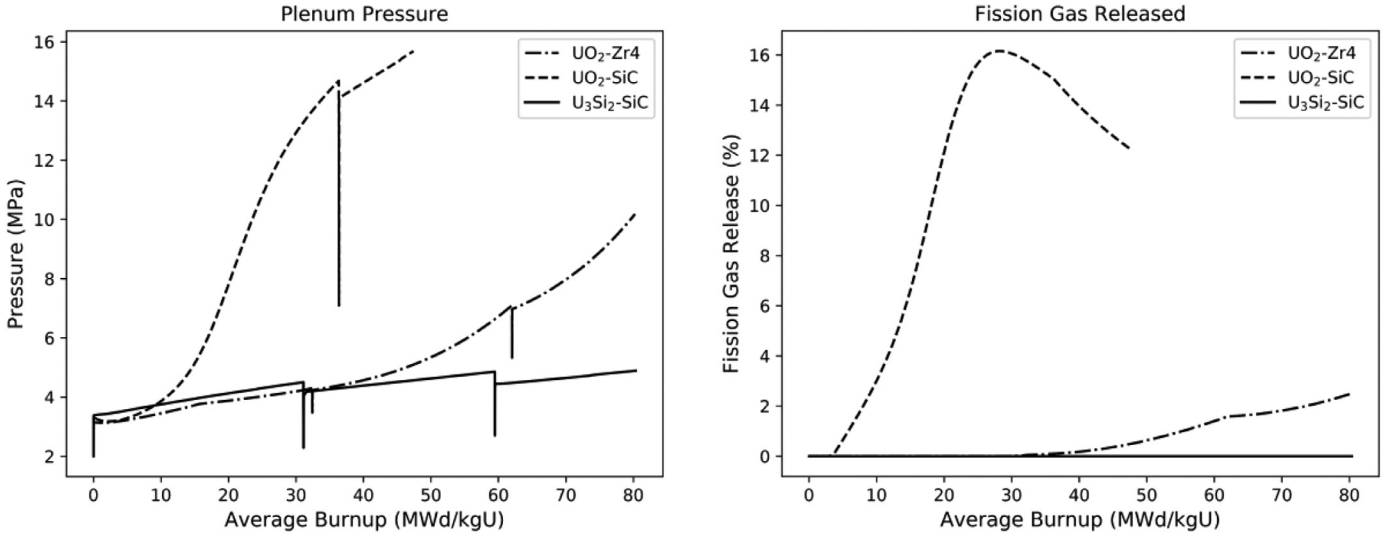

Fig. 6. Plenum pressure and fission gas release over average burnup.

FGR of U_3Si_2 is unknown, the Barani FGR model for U_3Si_2 provides FGR values similar to those established via post-irradiation examination at low burnup [5].

UO_2-SiC FGR is significantly higher than all others due to its excessively large temperature gradient. Considering the added risk of gas leakage due to microcracking in SiC, UO_2 is not recommended when paired with SiC cladding. In this respect, U_3Si_2 has the advantage, primarily due to its higher thermal conductivity that lowers average fuel temperatures at high burnup causing a decrease in the mobility of fission gasses. Importantly, the UO_2 fission gas model does not account for high-burnup structures and is not accurate past approximately 50 MWd/kgU. However, even at this moderate burnup, the improved FGR performance of U_3Si_2 is evident.

The reality of having essentially zero U_3Si_2 FGR is questionable at such high burnups. Such a result can be understood in terms of the model lacking certain physical phenomena, such as increased gas mobility, as a result of microcracking in the fuel or larger driving forces from fission-gas-degraded thermal conductivity. BISON UO_2 material models include these effects, which are partially responsible for its higher FGR. Since high burnup FGR data are unavailable for U_3Si_2, a FGR model coupled to cracking as well as thermal conductivity degradation would be a valuable addition to the simulation of U_3Si_2 performance in BISON.

Despite U_3Si_2 having a much lower FGR, the swelling model developed by Barani shows similarly low swelling. The present simulation indicates that U_3Si_2-SiC is expected to swell approximately half as much as UO_2-Zr4, which is in keeping with expectations set by post-irradiation examination at low burnups. As mentioned previously, the long-term effect of low FGR on fuel swelling in U_3Si_2 needs to be investigated further at higher burnup before such outcomes are to be believed.

4.3.3. Cladding hoop stress

Considering the vast material differences between CMC SiC and Zr4, the distribution of stress through the SiC cladding is expected to be uneven. Fig. 7 below indicates the maximum and minimum cladding hoop stresses over burnup for the three fuel combinations.

For the U_3Si_2-SiC and UO_2-SiC simulations, tensile stresses within the cladding are maintained within the SiC-SiC layer while the mSiC remains under compressive stress until contact occurs. This behavior is desirable since tensile strain of the mSiC layer

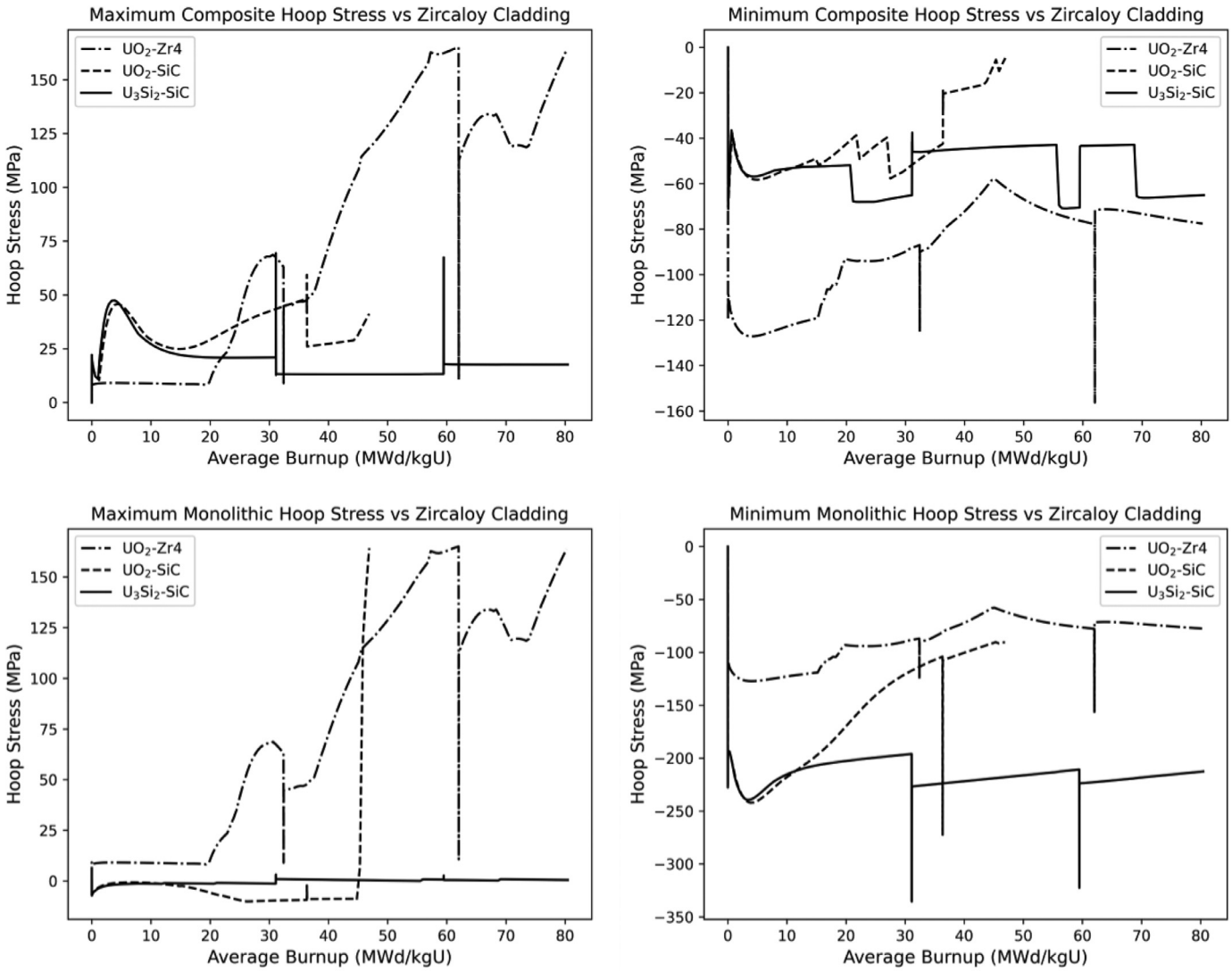

Fig. 7. Maximum and minimum cladding hoop stress over average burnup.

is a driving factor in microcracking, which has important implications for cladding hermeticity under load. Since the mSiC is maintained under compressive stress, Fig. 7 illustrates that tensile stress within the SiC-SiC cladding will increase greatly during shutdown. Although the mSiC remains under compressive load, the SiC-SiC layer is placed under tensile stresses exceeding 100 MPa. Considering that a round robin study of tubular CMC SiC properties indicates a PLS of about 92.8 MPa, cracking of the SiC-SiC is expected under normal operating conditions [42].

Fig. 7 makes it apparent that combinations of low thermal conductivity fuel and cladding, like UO_2-SiC, provide unacceptable performance under typical LWR conditions. This is especially true when the cladding is susceptible to brittle failure during PCMI. Additionally, although there is some minor fuel temperature benefit from the U_3Si_2-SiC fuel, there is no notable performance benefit in terms of cladding performance during normal operation.

4.4. Pellet cladding mechanical interaction

Due to the low power densities and temperatures for U_3Si_2-SiC, no PCMI was found to have occurred during the prior simulation. However, certain physical effects upon the fuel were not included as part of the simulation, such as radial fuel relocation caused by shuffling and inversion of the fuel rod between cycles. Because of this, insufficient stresses were created to evaluate conditions in which thermal creep of U_3Si_2 may be significant. Under such physical processes it is conceivable that despite U_3Si_2's relatively lower amount of fuel cracking, fragments of the fuel may relocate to create contact between the fuel and cladding.

To simulate such an occurrence, the relocation of a fragment of fuel into the fuel cladding gap is investigated by choosing an initial cladding gap of 30 μm to force PCMI to occur following the first cycle. In Fig. 8 below, maximum and average cladding stress demonstrate the pseudoelasticity of SiC-SiC during PCMI beginning at 40MWd/kgU. The stress distribution throughout PCMI is also provided and indicates that despite the mechanical compliance of SiC-SiC, the mSiC layer stress increases elastically until failure.

For U_3Si_2-SiC, rapid development of tensile stress within the cladding is evident during PCMI and causes a stress-based failure of the cladding near 48 MWd/kgU. Increases in both maximum and average hoop stress occur; however, maximum stresses are under a delay. Although contact occurs just before 40 MWd/kgU, a delay of approximately 3 MWd/kgU follows before maximum hoop stress begins to increase. This is in part due to the cracking compliance

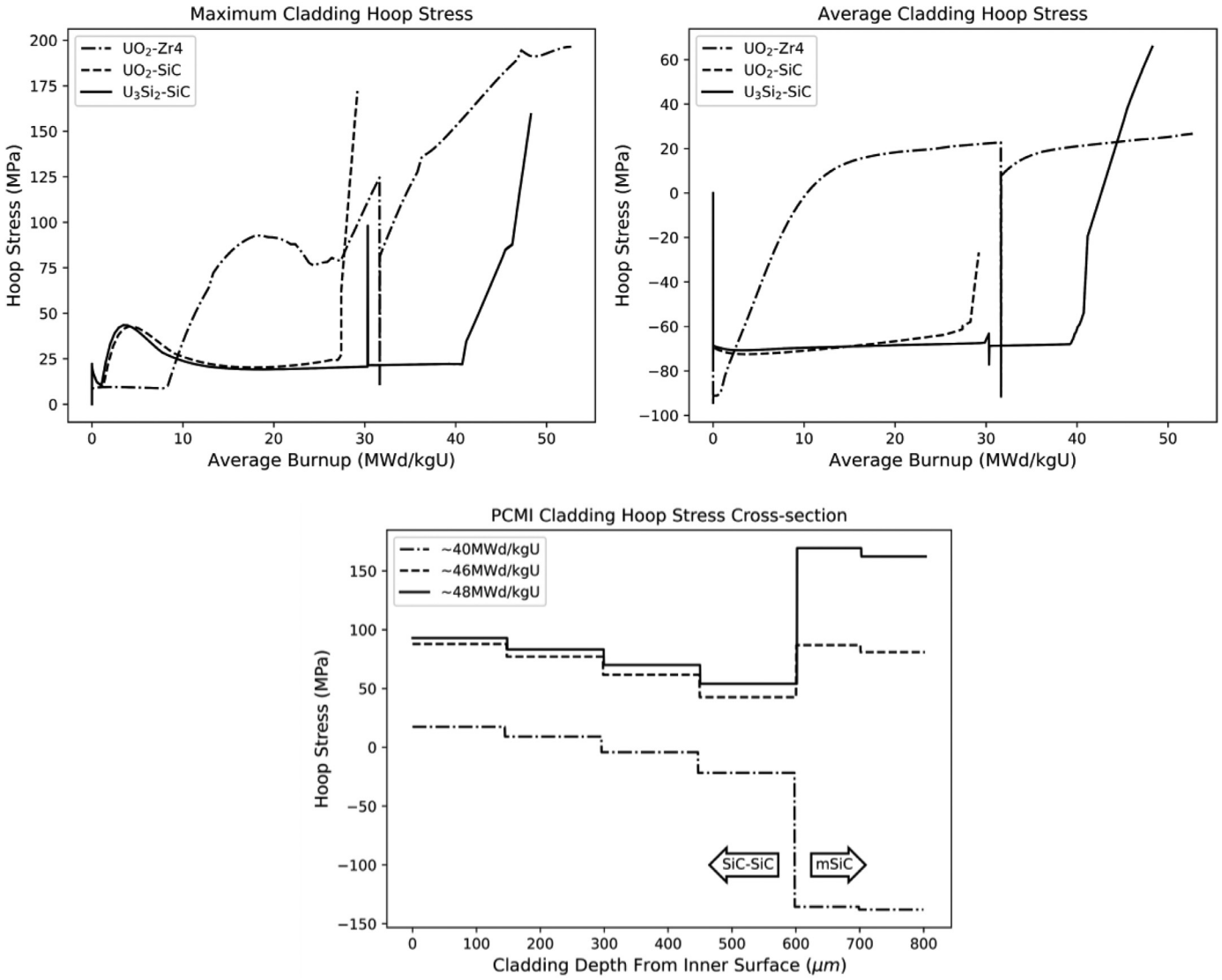

Fig. 8. Cladding hoop stress during simulated PCMI using a 30 μm cladding gap.

of the SiC-SiC layer evident in the decreasing slope of the average hoop stress in Fig. 8 near 40 MWd/kgU. The delay between contact and cladding failure is significant, which indicates that material design efforts to improve SiC-SiC compliance have an important role in preventing SiC cladding failure.

Of particular importance is the difference in cladding failure among UO_2-Zr4, UO_2-SiC, and U_3Si_2-SiC. PCMI for UO_2-Zr4 occurs through more than 40 MWd/kgU before failure; whereas, for U_3Si_2-SiC the cladding survives for less than 10 MWd/kgU. UO_2-SiC is the least compliant and the cladding fails within 4 MWd/kgU of contact. Regardless of the creep differences between UO_2 and U_3Si_2, the brittleness of SiC results in rapid failure of the cladding following PCMI for both UO_2-SiC and U_3Si_2-SiC.

In addition to using the 30 μm cladding gap, additional simulation cases were run for U_3Si_2-SiC using 0.1x, 1x, and 10x the nominal thermal creep rate for the model determined in Section 2. Nearly identical hoop stresses were obtained in each case, indicating that thermal creep of U_3Si_2 has little impact on mitigating cladding failure during PCMI. Given the low temperature in the fuel, thermal and irradiation creep of U_3Si_2 are low regardless of stress in the current model. Considering the BISON UO_2 thermal creep model is well understood, the rapid failure of SiC for both UO_2 and U_3Si_2 suggests that it is unlikely that creep of the fuel is capable of compensating for the brittle nature of SiC. Even with improved SiC-SiC layer compliance, stresses in the mSiC layer result in rapid failure of the cladding.

The reader is advised that the thermal creep model for U_3Si_2 was developed using compressive creep data between 25 and 78 MPa. As such, no experimental data were available to inform the development of the U_3Si_2 thermal creep model at fuel stresses that are typical during PCMI. Because of this, the creep behavior of U_3Si_2 at very high stresses is unknown and the PCMI behavior of U_3Si_2-SiC in Fig. 8 is an extrapolation subject to skepticism. Be that as it may, in light of the similarly rapid failure of UO_2-SiC for which creep is well understood, the PCMI behavior of U_3Si_2-SiC appears to be reasonable.

As discussed in Section 2.1, primary creep of U_3Si_2 is not included in the U_3Si_2 thermal creep model. Since primary creep would have a significant influence during the high stresses that occur during PCMI, there is substantial need for future experimental work to explore thermal creep of U_3Si_2 for stresses exceeding 100 MPa. Since U_3Si_2 has many metal-like properties, it may be that such a study would uncover significant creep during pellet cladding contact and improve the viability of U_3Si_2-SiC.

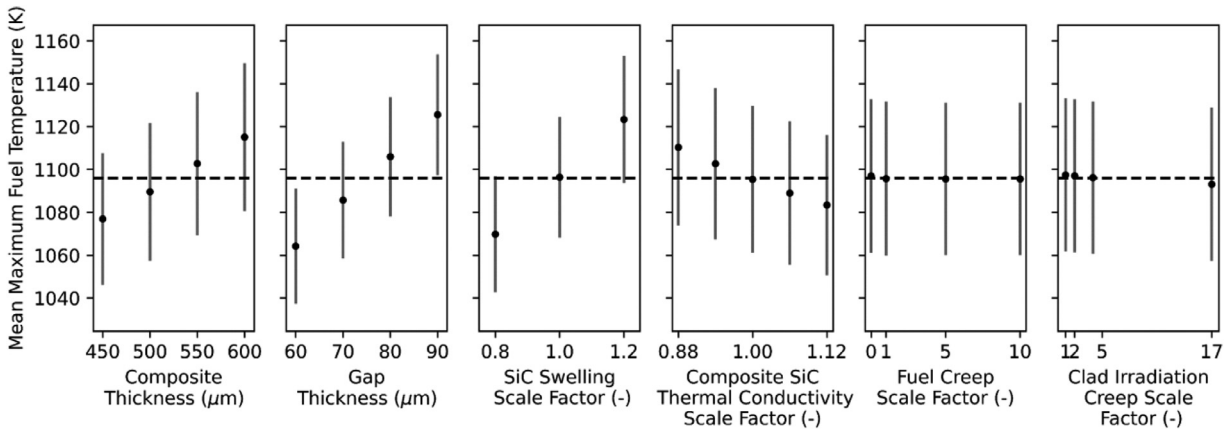

Fig. 9. Maximum fuel temperature response to variations in design parameters.

4.5. Multidimensional parameter study

4.5.1. Design parameter variations

The nominal parameter values used in the above analysis demonstrate the expected performance differences among UO_2-Zr4, UO_2-SiC, and U_3Si_2-SiC. However, despite the efforts involved in establishing the nominal case, it is expected that variations caused by uncertainties will exist in these parameters. Due to assumptions made while developing models for U_3Si_2 relocation, cracking, U_3Si_2 thermal creep, SiC monolithic and composite irradiation creep, and thermal conductivity, a variation study on these parameters was completed in combination with design variations in rod geometry due to cladding gap and composite thickness. Additionally, variations in SiC irradiative swelling were explored due to the large uncertainties in this model. Generally, the range of tested values for these parameters reflects the uncertainty in the experimental data from which the BISON models were derived.

Exactly 11,520 individual simulations were calculated to develop an understanding of the main effects that each parameter variation has on the simulation responses of maximum fuel temperature, cladding stress, cladding strain, and plenum pressure. The resulting plots of main effects demonstrate the average maximum value of each response with respect to every possible combination of parameter variations. This strategy allows succinct display of the mean maximum response value expected for any specified system parameter. As an indication of how much other parameter variations influence the response, error bars are displayed for one standard deviation above and below the average maximum calculated response.

Variations in composite thickness, gap thickness, composite SiC thermal conductivity, fuel creep, transient SiC irradiation creep, and SiC irradiation swelling are the parameter variations investigated in this study. The mSiC is maintained at a constant 0.2 mm as an environmental barrier layer to ensure complete hermeticity of the entire cladding package despite SiC-SiC cracking. Since lab scale SiC-SiC claddings have been produced with thicknesses as low as 350 μm [9], it is assumed that production of reliable SiC-SiC is possible at a thickness of 450 μm. Rod diameter is fixed in this parameter variation study so varying SiC-SiC thickness and cladding gap cause the pellet diameter to change accordingly.

The range in fuel creep scaling is somewhat arbitrary. However, due to the compressive nature of the experimental creep testing being opposite to the tensile creep found in LWR fuels, a factor of 10 is likely enough to capture this difference. $A \pm 12\%$ variation in SiC-SiC thermal conductivity represents uncertainties from experimental error and unexpected irradiation damage to the cladding. SiC-SiC transient irradiation creep is varied by a factor of up to 17 to account for the range of differences between BSR measurements and those found in-pile [37,38]. SiC irradiation swelling is explored over $a \pm 20\%$ variation.

In addition to the parameter variations discussed above, cases were run to test variations in fuel relocation and monolithic thermal conductivity. These were found to have a negligible impact on every response of interest and are omitted from the figures for the sake of brevity. In consideration of the power history used in this study, the main effects of the system parameter variations discussed below elucidate the range of expected performance of the U_3Si_2-SiC under low-power normal operation and should not be extended to high-power or accident conditions.

4.5.2. Fuel temperature and monolithic sic stress

As expected, Fig. 9 demonstrates that variations in SiC-SiC thermal conductivity, cladding gap, and SiC-SiC thickness have predictable effects on maximum fuel temperature. In other words, phenomena that improve thermal conductivity result in a lower mean maximum fuel temperature. In Fig. 9, the average maximum fuel temperature among 11,520 simulations show that very large changes in cladding thickness and cladding gap are possible with small changes to fuel temperature. However, the utility of main effects diagrams is found in selecting a design parameter that produces a specified system response to determine the constraints upon other design parameters.

For example, according to Fig. 9, if one desires a maximum fuel temperature of around 1050 K, a cladding gap of 60 μm might be chosen as a design parameter to achieve that goal. In Fig. 10, however, for a 60 μm cladding gap, there is significant variation in the mean maximum hoop stress in the monolithic cladding indicating that severe compromises in other design parameters would be necessary to maintain stress within the mSiC at an acceptable level. On the other hand, for a gap of 70 μm this variation in hoop stress is much smaller and allows more flexibility in choosing other design parameters. Further, a 70 μm gap thickness requires little compromise in fuel temperature.

Considering variations in mSiC hoop stress, generally a SiC-SiC thickness of less than 500 μm and cladding gaps of greater than 70 μm are recommended. In the absence of mechanical degradation, thermal conductivity variations have a small effect on fuel temperature. Despite this, SiC-SiC conductivity should not be allowed to degrade below the nominal case as hoop stress variations become significantly larger and additional compromises to other design parameters would be required to achieve adequately low stress within the mSiC cladding. This is especially true considering the additional loss of thermal conductivity that would occur due to mechanical damage [41]. In the ranges investigated in this

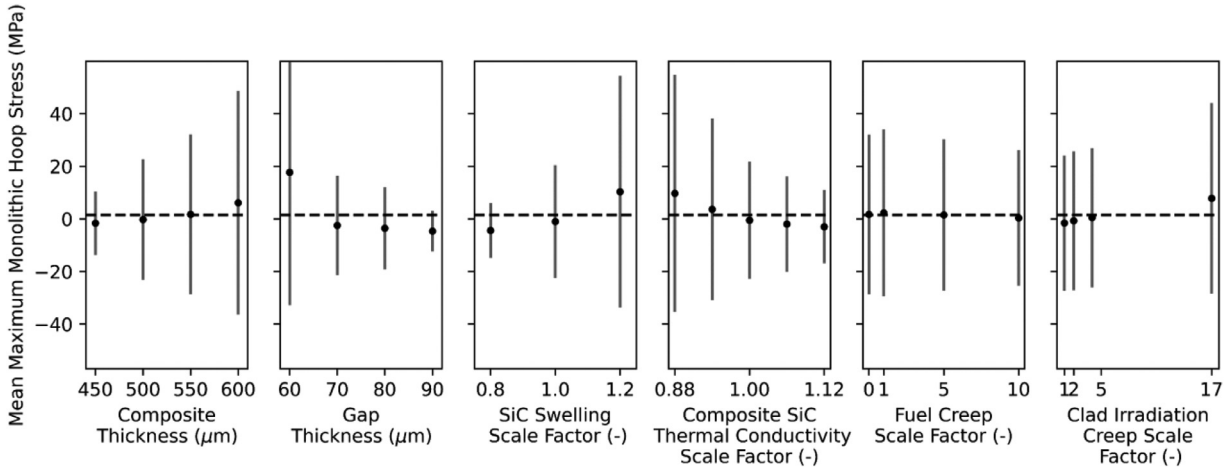

Fig. 10. Maximum mSiC hoop stress response to variations in design parameters.

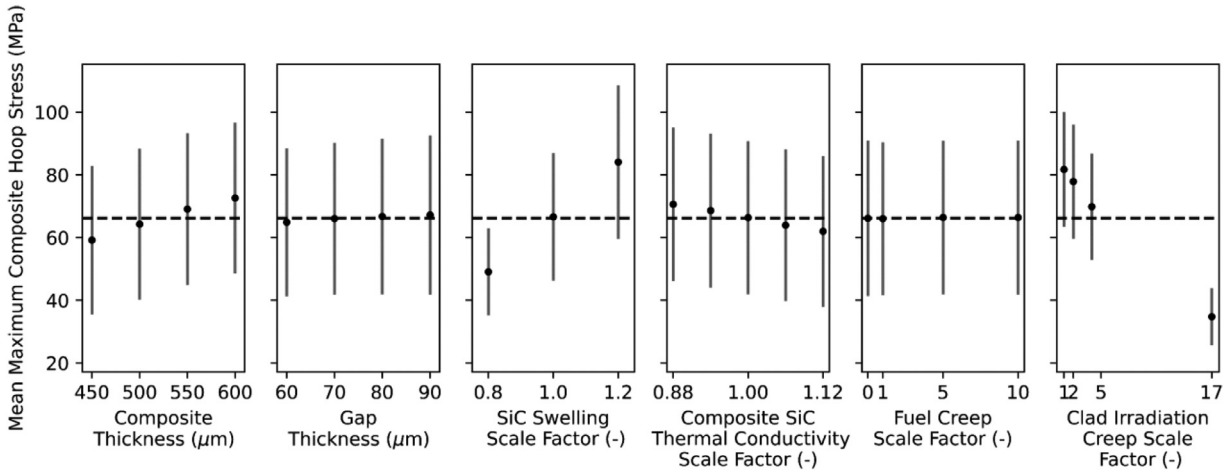

Fig. 11. Average of maximum SiC-SiC hoop stress response to variations in design parameters.

study, fuel thermal creep and cladding irradiation creep are negligible factors in terms of response variation and performance on mSiC hoop stress and fuel temperature. Indeed, with the exception of composite stress discussed below, thermal and irradiation creep was, on average, of minor influence on the various tested system responses.

4.5.3. Composite stress

In the literature, irradiation creep in SiC simulations has been considered small. This study applied a linear scale factor to the transient portion of SiC-SiC irradiation creep and found that, except for SiC-SiC hoop stress within the composite layer, irradiation creep is of little importance. Previous work indicates that irradiation creep will have a small deleterious effect on cladding stresses during PCMI [6]; however, for cases where the majority of simulations reach design burnup, the effect of irradiation creep can be ignored.

Apart from thin composite layers there are, on average, no parameter combinations that prevent hoop stresses that will exceed the SiC-SiC PLS and induce cracking. This is especially true in the near-nominal irradiation creep cases. Fig. 11 emphasizes the importance of improving knowledge of SiC irradiation swelling as it has the largest impact on the mean SiC-SiC hoop stresses attained. Additional experimentation to reduce uncertainty within this model would certainly be valuable.

5. Conclusion

Thermal creep follows the Mukherjee-Bird-Dorn relationship of Eq. (2) along with the creep parameters of Table 2 for stresses between 25 and 78 MPa, and temperatures between 1121 K to 1274 K, in U_3Si_2 pellets fabricated by INL circa 2016. U_3Si_2 thermal creep was calculated to be very small during nominal simulation conditions, even in the 10x nominal case. In the nominal simulation, pellet clad contact was completely avoided through an average burnup of 80MWd/kgU indicating that SiC cladding would be mechanically viable for use with high thermal conductivity fuels during normal operating conditions and low power density. Performance of U_3Si_2-SiC at high power density and during PCMI is very poor. UO_2-SiC underperformed in every metric, emphasizing the importance of avoiding combinations of SiC with low thermal conductivity fuels.

Since U_3Si_2 operates at very low temperatures, it shows little sensitivity to design parameter variations except fuel to cladding gap, SiC-SiC layer thickness, and SiC irradiation swelling. Fuel creep has little influence on reducing the cladding stress due to PCMI. Thus, because the SiC cladding has little ductility, premature PCMI failures can readily occur if the fuel comes in contact with the cladding. Hence, fragment relocation during fuel shuffling, or dislodged pellet chips introduced during manufacture are of particular concern to this fuel concept.

Considering these outcomes, a composite layer thickness of less than 500 μm and a cladding gap of greater than 70 μm is recommended in U_3Si_2-SiC fuel designs. Strategies to minimize composite layer thickness without compromising monolithic layer hermeticity are of greatest interest to this concept fuel as they have the largest impact on heat transfer and can prevent fuel cladding contact. Strategies to prevent extreme mechanical degradation of SiC-SiC thermal conductivity will be necessary to prevent failure of mSiC. Further experimental studies are needed to establish thermal creep of U_3Si_2 under the high stress conditions of PCMI. Experimental validation of high burnup U_3Si_2-SiC PCMI is also needed. In the absence of these data, U_3Si_2 creep compliance appears to be insufficient to accommodate the brittle nature of mSiC during PCMI even with the pseudoplastic enhancement of an inner layer of SiC-SiC. Prior to use as a LWR fuel, U_3Si_2-SiC requires experimental confirmation where fuel-cladding contact may occur due to excesses in power density or burnup.

Declaration of Competing Interest

The authors declare that they have no known competing financial interests or personal relationships that could have appeared to influence the work reported in this paper.

CRediT authorship contribution statement

J.A. Yingling: Writing - original draft, Conceptualization, Methodology, Software, Formal analysis. **K.A. Gamble:** Methodology, Writing - review & editing, Resources, Visualization. **Elwyn Roberts:** Methodology, Supervision. **R. Austin Freeman:** Conceptualization, Software, Investigation, Data curation. **Travis W. Knight:** Conceptualization, Supervision, Project administration, Funding acquisition.

Acknowledgements

This research was performed using funding received from the DOE Office of Nuclear Energy's Nuclear Energy University Programs; and the Nuclear Regulatory Commission fellowship program. The manuscript has been authored by a contractor of the U.S. Government under Contract DE-AC07–05ID14517. Accordingly, the U.S. Government retains a non-exclusive, royalty free license to publish or reproduce the published form of this contribution, or allow others to do so, for U.S. Government purposes.

References

[1] J.J. Powers, Early Implementation of SiC Cladding Fuel Performance Models in BISON, Oak Ridge National Laboratory, Oak Ridge, 2015.
[2] V. Kocevski, D.A. Lopes, A.J. Claisse, T.M. Besmann, Understanding the interface interaction between U3Si2 fuel and SiC cladding, Nat Commun 11 (2020) 2621.
[3] B.W. Gong, T.K. Yao, P.H. Lei, J. Harp, A.T. Nelson, J. Lian, Spark plasma sintering (SPS) densified U3Si2 pellets: microstructure control and enhanced mechanical and oxidation properties, J Alloys Compd 825 (2020) 154022.
[4] A.M. Ward, M. Wang, M. Neumann, M. Memmott, A. Manera, T.J. Downar, A simulation of I2S-LWR selected transients, Ann Nucl Energy 145 (2020) 105421.
[5] F. Cappia, J.M. Harp, Postirradiation examinations of low burnup U3Si2 fuel for light water reactor applications, Journal of Nuclear Materials (2019) 62–79.
[6] J.A. Yingling, Bison Simulation-Based Identification of Important Design Criteria for U3Sl2 Fuels With Composite-Monolithic Duplex SiC Cladding, Scholar Commons, Columbia, 2019.
[7] E.A.C. Mercado, High Temperature Compression Creep of U3Si2, University of South Carolina, Columbia, 2018.
[8] A. Oizumi, H. Akie, N. Iwamoto, T. Kugo, Evaluation of neutron economical effect of new cladding materials in light water reactors, J Nucl Sci Technol 51 (2014) 77–90.
[9] J.D. Stempien, D.M. Carpenter, G. Kohse, M. Kazimi, Characteristics of Composite Silicon Carbide Fuel Cladding after Irradiation under Simulated PWR Conditions, Nucl Technol 183 (1) (2013) 13–29.
[10] K.E. Metzger, Analysis of Pellet Cladding Interaction and Creep of U3Si2 Fuel for Use in Light Water Reactors, University Of South Carolina, Columbia, 2016.
[11] Y. He, K. Shirvan, Y. Wu, G.H. Su, Fuel performance optimization of U3Si2-SiC design during normal, power ramp and RIA conditions, Nuclear Engineering and Design 353 (2019) 110276.
[12] L. Wei, S. Koroush, U3Si2-SiC fuel performance analysis in BISON during normal operation, Ann Nucl Energy 132 (2019) 34–45.
[13] C.H. Bumgardner, F.M. Heim, D.C. Roache, A. Jarma, P. Xu, R. Lu, E. Lahoda, B.P. Croom, C.P. Deck, X. Li, Unveiling hermetic failure of ceramic tubes by digital image correlation and acoustic emission, Journal of the American Ceramic Society (2019) 1–14.
[14] M.R. Finlay, G.L. Hofman, J.L. Snelgrove, Irradiation Behavior of Uranium Silicide Compounds, Journal of Nuclear Materials 325 (2–3) (2004) 118–128.
[15] T.W. Knight, "U3Si2 Fabrication and Testing for Implementation into the BISON Fuel Performance Code," DOI: 10.2172/1434631, 2018.
[16] M.A. Meyers, K.K. Chawla, Mechanical Behavior of Materials, Cambridge University Press, Cambridge, 2009.
[17] C.F. Terrapin, "Unpublished Work," 2018.
[18] C. Terrapin, J. McCreary, Internal Communication on Unpublished Work, University of South Carolina, 2019.
[19] A. Cheniour, M.R. Tonks, B. Gong, T. Yao, L. He, J. Harp, B. Beeler, Y. Zhang, J. Lian, Development of a grain growth model for U3Si2 using experimental data, phase field simulation and molecular dynamics, Journal of Nuclear Materials 532 (2020) 152069.
[20] K.A. Gamble, A.F. Williams, P.K. Chan, A Three-dimensional Analysis of the Local Stresses and Strains at the Pellet Ridges in a Horizontal Nuclear Fuel Element, in: Proceedings of the 22nd International Conference on Nuclear Engineering, 2014.
[21] J.D. Hales, R.L. Williamson, S.R. Navascone, D.M. Perez, B.W. Spencer, G. Pastore, Multidimensional multiphysics simulation of TRISO particle fuel, Journal of Nuclear Materials 443 (1–3) (2013) 531–543.
[22] E.G. Obbard, K.D. Johnson, P.A. Burr, D.A. Lopes, D.J. Gregg, K.D. Liss, G. Griffiths, N. Scales, S.C. Middleburgh, Anisotropy in the Thermal Expansion of Uranium Silicide Measured by Neutron Diffraction, Journal of Nuclear Materials 508 (2018) 516–520.
[23] Y. Katoh, K. Ozawa, C. Shih, T. Nozawa, R.J. Shinavski, A. Hasegawa, L.L. Snead, Continuous SiC Fiber, CVI SiC Matrix Composites for Nuclear Applications: properties and Irradiation Effects, Journal of Nuclear Materials 488 (2014) 448–476.
[24] A. Marion, "Safety Evaluation by the Office of Nuclear Reactor Regulation of Electric Power Research Institute," 13 June 2006. [Online]. Available: https://www.nrc.gov/docs/ML0616/ML061650107.pdf. [Accessed 3 September 2020].
[25] J.T. White, Update to the U3Si2 Property Handbook, Los Alamos National Laboratory, Los Alamos, 2018.
[26] J.G. Stone, R. Schleicher, C.P. Deck, G.M. Jacobsen, H.E. Khalifa, C.A. Back, Stress Analysis and Probabilistic Assessment of Multi-Layer SiC-Based Accident Tolerant Nuclear Fuel Cladding, Journal of Nuclear Materials 466 (2015) 682–697.
[27] T. Koyanagi, Y. Katoh, G. Jacobsen, C. Deck, Handbook of LWR SiC/SiC Cladding Properties - Rev 1, Oak Ridge National Laboratory, 2018.
[28] G. Pastore, L. Luzzi, V.D. Marcello, P.V. Uffelen, Physics-based modelling of fission gas swelling and release in UO2 applied to integral fuel rod analysis, Nuclear Engineering and Design 256 (2013) 75–86.
[29] T. Barani, G. Pastore, D. Pizzocri, C. Matthews, A. Alfonsi, K.A. Gamble, P.V. Uffelen, L. Luzzi and J.D. Hales, "Multiscale modeling of fission gas behavior in U3Si2 under LWR conditions".
[30] G.L. Hofman, Crystal Structure Stability and Fission Gas Swelling in Intermetallic Uranium Compoints, Journal of Nuclear Materials 140 (3) (1986) 256–263.
[31] Y. Katoh, T. Koyanagi, J.L. McDuffee, L.L. Snead, K. Yueh, Dimensional Stability and Anisotropy of SiC and SiC-Based composites in Transition Swelling Regime, Journal of Nuclear Materials 499 (2018) 471–479.
[32] D.G. Franklin, Zircaloy-4 cladding deformation during power reactor irradiation, Zirconium in the Nuclear Industry, ASTM International, 1982.
[33] L.L. Snead, T. Nozawa, Y. Katoh, T.S. Byun, S. Kondo, D.A. Petti, Handbook of SiC Properties for Fuel Performance Modeling, Journal of Nuclear Materials 371 (2007) 329–377.
[34] G. Singh, K. Terrani, Y. Katoh, Thermo-mechanical assessment of full SiC/SiC composite cladding for LWR applications with sensitivity analysis, Journal of Nuclear Materials 499 (2018) 26–143.
[35] J. Braun, C. Sauder, J. Lamon, F. Balbaud-Célérier, Influence of an original manufacturing process on the properties and microstructure of SiC/SiC tubular composites, Composites Part A 123 (2019) 170–179.
[36] C.M. Allison, G.A. Berna, R. Chambers, E.W. Coryell, K.L. Davis, D.L. Hagrman, N.L. Hampton, J.K. Hohhorst, R.E. Mason, M.L. McComas, K.A. McNeil, R.L. Miller, C.S. Olsen, G.A. Reymann, L.J. Siefken, SCDAP/RELAP5/MOD3.1 Code Manual, Volume IV: MATPRO– A Library of Materials Properties For Light-Water-Reactor Accident Analysis, Idaho National Engineering Laboratory, 1993.
[37] T. Koyanagi, Y. Katoh, K. Ozawa, K. Shimoda, T. Hinoki, L.L. Snead, Neutron-irradiation creep of silicon carbide materials beyond the initial transient, Journal of Nuclear Materials 478 (2016) 97–111.
[38] T. Koyanagi, K. Terrani, T. Karlsen, V. Andersson, D. Sprouster, L. Ecker, Y. Katoh, In-pile tensile creep of chemical vapor deposited silicon carbide at 300C, Journal of Nuclear Materials 521 (2019) 63–70.
[39] N.E. Hoppe, Engineering model for ziraloy creep and growth, in: Proceedings of the ANS-ENS International Topical Meeting on LWR Fuel Performance, Avignon, France, 1991, pp. 157–172.
[40] R.B. Fancher, I.B. Fiero, H. Freeburn, A.M. Garde, M.W. Kennard, M.A. Krammen, P.G. Smerd, N.T. Yackle, ESCORE: the EPRI Steady-State Core Reload Evaluator Code, Oak Ridge National Laboratory, Oak Ridge, 1987.

[41] W. Li, K. Shirvan, U3Si2-SiC fuel performance analysis in BISON during normal operation, Ann Nucl Energy 132 (2019) 34–45.
[42] G. Singh, S. Gonczy, C. Deck, E. Lara-Curzio, Interlaboratory round robin study on axial tensile properties of SiC-SiC CMC tubular test specimens, International Journal of Applied Ceramic Technology (2018) 1334–1349.
[43] G. Singh, T. Koyanagi, C. Petrie, C. Deck, K. Terrani, J.D. Arregui-Mena, Y. Katoh, Elastic moduli reduction in SiC-SiC tubular specimen after high heat flux neutron irradiation measured by resonant ultrasound spectroscopy, Journal of Nuclear Materials 523 (2019) 391–401.
[44] C.A. Lewinsohn, M.L. Hamilton, G.E. Youngblood, R.H. Jones, F.A. Garner, S.L. Hecht, A. Kohyama, Irradiation-enhanced creep in SiC: data summary and planned experiments, Journal of Nuclear Materials (1998) 36–46.
[45] B.M. Adams, W.J. Bohnhoff, K.R. Dalbey, M.S. Edeida, J.P. Eddy, M.S. Eldred, G. Geraci, R.W. Hooper, P.D. Hough, K.T. Hu, J.D. Jakeman, M. Khalil, K.A. Maupin, J.A. Monschke, E.M. Ridgway, A.A. Rushdi, J.A. Stephens, L.P. Swiler, D.M. Vigil, T.M. Wildey, J.G. Winokur, Dakota, a Multilevel Parallel Oject-Oriented Framework For Design optimization, Parameter Estimation,Uncertainty quantification, and Sensitivity Analysis, Sandia National Laboratory, Albuquerque, 2014.
[46] G. Pastore, L.P. Swiler, J.D. Hales, S.R. Novascone, D.M. Perez, B.W. Spencer, L. Luzzi, P.V. Uffelen, R.L. Williamson, Uncertainty and sensitivity analysis of fission gas behavior in engineerin-scale fuel modeling, Journal of Nuclear Materials 456 (2015) 398–408.
[47] K.A. Gamble, Investigation of Coated Cladding Ballooning Behavior Using BISON, TopFuel, Seattle, 2019.
[48] R.L. Williamson, K.A. Gamble, D.M. Perez, S.R. Navascone, G. Pastore, R.J. Gardner, J.D. Hales, W. Liu, A. Mai, Validating the BISON fuel performance code to integral LWR experiments, Nuclear Engineering and Design 301 (2016) 232–244.
[49] R.L. Williamson, G. Pastore, B.W. Spencer, J.D. Hales, T. Tverberg, BISON Validation for LOCA and PCMI Behavior Using Measurements From the Halden Reactor Project, Idaho National Laboratory, 2017.
[50] N.E. Todreas, M.S. Kazimi, Nuclear Systems: Volume 1, 2nd Edition, CRC Press, Boca Raton, 2011.
[51] C. Hove, "24-month PWR fuel cycles - Two decades of AREVA design and operating experience," 2015.
[52] M. Do, X.H. Nguyen, S. Jang, Y. Kim, Physics study for high-performance and very-low-boron APR1400 core with 24-month cycle length, Nuclear Engineering and Technology 52 (5) (2020) 869–877.
[53] J.R. Burns, R. Hernandez, K.A. Terrani, A.T. Nelson, R.B. Nicholas, Reactor and fuel cycle performance of light water reactor fuel with U235 enrichments above 5%, Ann Nucl Energy 142 (2020) 107423.
[54] Nuclear Energy Agency, Very High Burn-ups in Light Water Reactors, OECD, 2006.
[55] Y. Deng, S. Koroush, W. Yingwei, S. Guanghui, Probabilistic view of SiC/SiC composite cladding failure based on full core thermo-mechanical response, Journal of Nuclear Materials 507 (2018) 24–37.
[56] L.O. Jernkvist, Prediction of Failure of Highly Irradiated Zircaloy Clad Tubes under Reactivity Initiated Accidents, in: Transactions of the 17th Internation Conference on Structural Mechanis in Reactor Technology, Prague, 2003.
[57] G. Singh, R. Swet, N.R. Brown, B.D. Wirth, Y. Katoh, K. Terrani, Parametric Evaluation of SiC/SiC composite Cladding with UO2 Fuel for LWR Applications: fuel Rod Interactions and Impact of Nonuniform Power Profile in Fuel Rod, Journal of Nuclear Materials 499 (2018) 155–167.